

Glauber modeling of high-energy nuclear collisions at sub-nucleon level

C. Loizides¹

¹*Lawrence Berkeley National Laboratory, Berkeley, California, USA*

Glauber models based on nucleon–nucleon interactions are commonly used to calculate properties of the initial state in high-energy nuclear collisions, and their dependence on impact parameter or number of participating nucleons. In this article, an extension of the Glauber model to any number of constituents is presented. Properties of the initial state, such as the number of constituent participants and collisions, as well as eccentricity and triangularity, are calculated and systematically compared for different assumptions to distribute the sub-nuclear degrees of freedom and for various collision systems. The code for the constituent Monte Carlo Glauber program is made publicly available.

I. INTRODUCTION

Properties of the initial state in high-energy nuclear collisions are commonly calculated using a Glauber model [1]. In these calculations, nuclei are composed out of a set of nucleons, and the nuclear reaction is approximated by successive independent nucleon–nucleon (NN) interactions assuming the nucleons travel in a straight line along the beam axis (eikonal approximation). The so called “optical” Glauber calculations [2, 3] assume a smooth matter density distribution for the makeup of the nuclei, while the Monte Carlo (MC) based models [4, 5] distribute individual nucleons event-by-event, and collision properties are obtained by averaging over multiple events. In both cases, usually one uses a Fermi distribution for the radial direction and a uniform distribution for the solid angle.

These calculations have been extended to sub-nucleon level by taking into account three valence quarks per nucleon in the collision process [6]. It has recently been shown [6–10], that particle production at mid-rapidity in high-energy nucleus–nucleus collisions scales almost linearly with the number of quark participants, without the need to introduce a contribution from a hard-scattering component scaling with the number of binary nucleon–nucleon collisions. Further interest in such extensions arises since understanding the observed azimuthal momentum anisotropy from the spatial anisotropy of the initial state in pA and even pp collisions needs calculations of the initial state in small systems at sub-nucleon level [11].

In this article, an extension of the Glauber MC model to any number of constituents, i.e. sub-nucleon degrees of freedom, is presented. In Sec. II the standard Glauber MC model is briefly recalled, while in Sec. III its extension to sub-nucleon level is discussed. Section. IV discusses properties of the initial state, such as the number of constituent participants and collisions, as well as eccentricity and triangularity, calculated for a variety of different assumptions to distribute the sub-nuclear degrees of freedom and for various collision systems. The code for the constituent MC Glauber program is described in App. A. Additional calculations of the overlap area and participant density are discussed in App. B.

Nucleus	R [fm]	R_s [fm]	a [fm]	a_s [fm]
¹⁹⁷ Au	6.38 ± 0.13	6.42	0.535 ± 0.053	0.44
²⁰⁸ Pb	6.62 ± 0.06	6.65	0.546 ± 0.010	0.46

TABLE I: Standard and rescaled charge-density parameters.

$\sqrt{s_{NN}}$ [TeV]	0.019	0.2	2.76	5.02	7	13
σ_{NN} [mb]	33	42	64	70	74	78

TABLE II: Values used for σ_{NN} at various $\sqrt{s_{NN}}$.

II. MC GLAUBER CALCULATION

The Glauber calculation of a nucleus–nucleus collision is done as described in Ref. [12]. First, the positions of each of the A nucleons in a nucleus are determined according to the measured charge density distribution of the nucleus extracted from low-energy electron scattering experiments [13]. For spherical nuclei, such as Pb, the distribution is taken to be uniform in azimuthal and polar angles, and a two-parameter Fermi function

$$\rho(r) = \rho_0 \left(1 + \exp \left(\frac{r - R}{a} \right) \right)^{-1} \quad (1)$$

in the radial direction. In Eq. 1, R is the nuclear radius, and a is the skin depth, and the overall normalization ρ_0 is not relevant for the calculation. To mimic a hard-core repulsion potential in the context of the MC Glauber model, one usually requires a minimum inter-nucleon separation (d_{\min}) of 0.4 fm between the centers of the nucleons. These excluded-volume effects of the nucleons distort the resulting nuclear density and can be absorbed by rescaling the charge-density parameters [14]. The standard and rescaled values for Au and Pb nuclei are given in Tab. I, for other nuclei see Ref. [15].

Second, the collision impact parameter (b) is determined from $dN/db \propto b$, and the centers of the nuclei are shifted to $(-b/2, 0, 0)$ and $(b/2, 0, 0)$ ¹. Following the

¹ The reaction plane, i.e. the plane defined by the impact param-

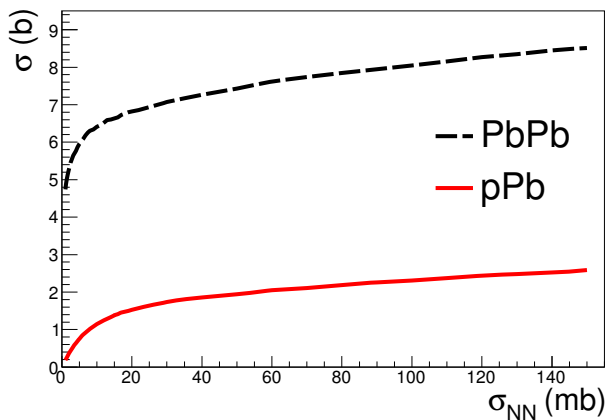


FIG. 1: Calculated total cross sections for PbPb and pPb collisions as a function of σ_{NN} .

eikonal ansatz, the nucleons are assumed to move along a straight trajectory along the beam axis. Their transverse positions are held constant during the short passage time of the two high-energy nuclei, while their longitudinal coordinate does not play a role in the calculation. The nuclear reaction is modeled by successive independent interactions between two nucleons from different nuclei. The interaction strength between two nucleons is parameterized by the nucleon–nucleon inelastic cross section (σ_{NN}). Two nucleons from different nuclei are supposed to collide if their relative transverse distance is less than

$$D = \sqrt{\sigma_{NN}/\pi}. \quad (2)$$

A nucleus–nucleus collision is accepted if at least one such nucleon–nucleon collision was obtained. The values used for σ_{NN} are usually obtained from the difference of total and elastic pp cross section measurements [16–18], and are summarized in Tab. II for a number of collision energies.

To estimate systematic uncertainties for calculated quantities one should systematically modify the parameters of the calculation [12]. One typically varies the parameters of the nuclear density profile within the measured 1σ uncertainties, the minimum inter-nucleon separation distance by 100%, and the σ_{NN} by about ± 3 mb and ± 5 mb at RHIC and LHC, respectively.

The Glauber calculation gives $\sigma_{PbPb}^{MC} = 7.6 \pm 0.2$ b and $\sigma_{pPb}^{MC} = 2.1 \pm 0.1$ b for the total PbPb and pPb cross sections, in good agreement with the measured values of $\sigma_{PbPb} = 7.7 \pm 0.6$ b at $\sqrt{s_{NN}} = 2.76$ TeV [19] and $\sigma_{pPb} = 2.06 \pm 0.08$ b at $\sqrt{s_{NN}} = 5.02$ TeV [20], respectively. For PbPb at $\sqrt{s_{NN}} = 5.02$ a total cross section of $\sigma_{PbPb}^{MC} = 7.7 \pm 0.2$ b is predicted. The total cross sections of PbPb and pPb as a function of σ_{NN} are shown in Fig. 1

eter and the beam direction, is given by the x - and z -axes, while the transverse plane is given by the x - and y -axes.

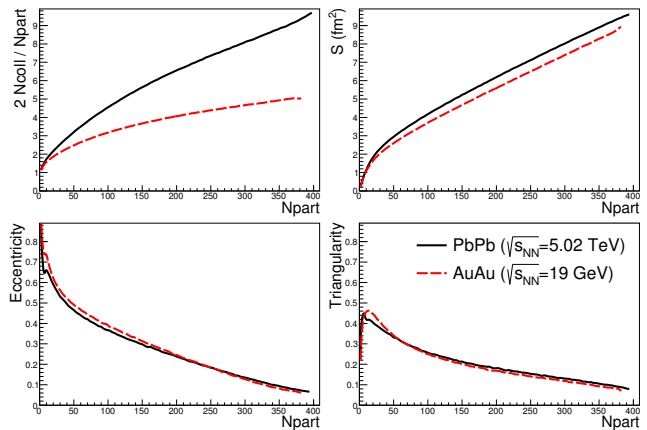


FIG. 2: Geometric properties computed with Glauber MC for AuAu collisions at $\sqrt{s_{NN}} = 19$ GeV and PbPb collisions at $\sqrt{s_{NN}} = 5.02$ TeV.

calculated using the central values of the parameters (i.e. without systematic uncertainties, which would be about 3 and 8%, respectively).

MC Glauber calculations are typically used to compute geometrical properties of the collision, such as the number of participating nucleons in the collision, N_{part} , i.e. the number of nucleons that are hit at least once, or the number of independent nucleon–nucleon collisions, N_{coll} , i.e. the total number of collisions between nucleons. Particle production at low p_T roughly scales with N_{part} [21], while hard processes are found to scale with N_{coll} [22–24]. Examples of geometrical properties are shown in Fig. 2. The ratio between N_{coll}/N_{part} normalized to that of pp (i.e. 1/2), which has been argued to be a measure for the relative importance of hard versus soft processes, rises with centrality and in particular with collision energy. The overlap area of the two colliding nuclei is proportional to $S = \sqrt{\sigma_x^2 \sigma_y^2 - \sigma_{xy}^2}$, given by the (co-)variances of the participant distributions in the transverse plane [12]. The area can also be directly computed from the MC as explained in App. B, leading to a slightly different shape.

The eccentricity [25] and triangularity [26] of the collision region, given by $\varepsilon_i = \langle r^i \cos(i\phi - i\psi_i) \rangle / \langle r^i \rangle$ [27], characterize the initial geometrical shape. These properties are similar between AuAu and PbPb collisions, and at different energies.

III. EXTENSION TO SUB-NUCLEON LEVEL

The calculation can be readily extended to sub-nucleon level by assuming that a nucleon carries N_c degrees of freedom. Often $N_c = 3$ for three constituent quarks [6–8], but larger numbers (up to $N_c = 17$) have previously [28] been used to account for the effective number of partonic degrees of freedom. Generalizing Eq. 2, the interaction

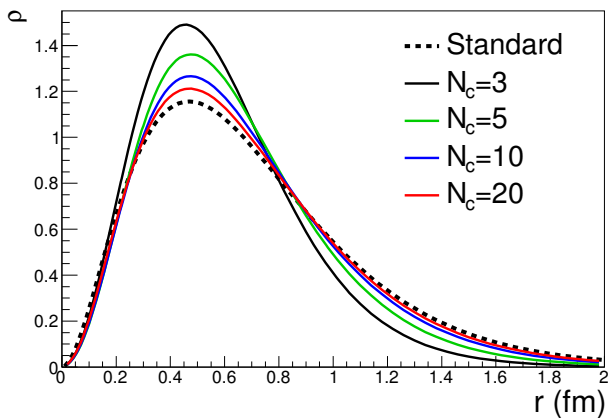


FIG. 3: Radial distribution of constituents after recentering when constructed from the standard parameterization (Eq. 4) for different N_c .

between two constituents can be modeled by an effective parton-parton cross section (σ_{cc}) in the same way as before, i.e. two constituents from different nuclei collide if their relative transverse distance is less than

$$D = \sqrt{\sigma_{cc}/\pi}. \quad (3)$$

There are two, somewhat limiting, cases to distribute sub-nucleon degrees of freedom. The first is to bind constituents to nucleons making up the nucleus (labeled as “bound” in figures). In this case, N_c constituents are radially distributed centered around each nucleon according to

$$\rho(r) = \exp(-r/R) \quad (4)$$

with $R = 0.234$ fm based on the measured form factor of the proton [29]. The second is to freely distribute constituents over the whole nucleus (labeled as “free” in figures). In this case $A \times N_c$ constituents are distributed according to Eq. 1.² In both cases, a hard core repulsion potential is not considered.

When the constituents are bound to nucleons, recentering of the constituents to align with the centers of their respective nucleons, introduces a distortion of the resulting radial constituent distribution. The effect is most dramatic for $N_c = 3$, and reduces quickly with increasing number of constituents as shown in Fig. 3. For $N_c = 3$, the distortion can be avoided by distributing the constituents according to an empirically determined function [8]

$$\rho(r) = r^2 \exp(-r/R) \times \left[(1.22 - 1.89r + 2.03r^2) \right. \\ \left. (1 + 1/r - 0.03/r^2)(1 + 0.15r) \right] \quad (5)$$

² This is conceptually similar to the optical approach originally used in Ref. [6].

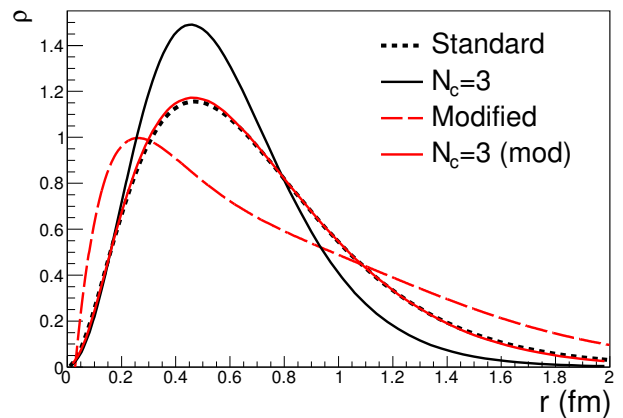


FIG. 4: Radial distribution of constituents after recentering when constructed from the standard (Eq. 4) or modified (Eq. 5) parameterizations for $N_c = 3$.

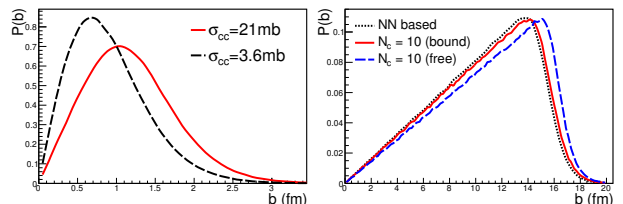


FIG. 5: Impact parameter distribution for pp (left) and PbPb (right) collisions. In case of pp, $\sigma_{cc} = 3.6$ and 21 mb with $N_c = 3$ are used for pp collisions at $\sqrt{s} = 0.2$ and 7 TeV, respectively. For PbPb collisions at $\sqrt{s_{NN}} = 5.02$ TeV, the standard nucleon-based approach is compared to bound and freely-distributed cases using $\sigma_{cc} = 3$ mb and $N_c = 10$.

as shown in Fig. 4. Equation 5 holds for $N_c = 3$. Hence, it is used as an alternative to Eq. 4 only in the case of constraining constituents to nucleons. This case is labeled as “mod” when displayed in figures. If not otherwise specified in the following, we do not recenter the constituents. In any case, not recentering has a negligible effect on the center of a nucleus since the deviations from the center-of-mass average out over AN_c degrees of freedom.

Example impact parameter distributions are shown in Fig. 5 for pp collisions at $\sqrt{s} = 0.2$ and 7 TeV in the left, and for PbPb collisions at $\sqrt{s_{NN}} = 5.02$ TeV in the right panel. In the case of pp, the distributions are obtained using $\sigma_{cc} = 21$ and 3.6 mb for $N_c = 3$, and extend beyond the hard-sphere limit of about 1.0 and 1.5 fm, respectively. In the case of PbPb, the distribution obtained for the standard NN based approach is compared to the bound and freely-distributed cases for $\sigma_{cc} = 3$ mb and $N_c = 10$. Freely-distributing constituents instead of binding them into nucleons generally leads to a wider impact parameter distribution.

Nuclear reaction cross sections can be computed by counting if there was at least one collision among two

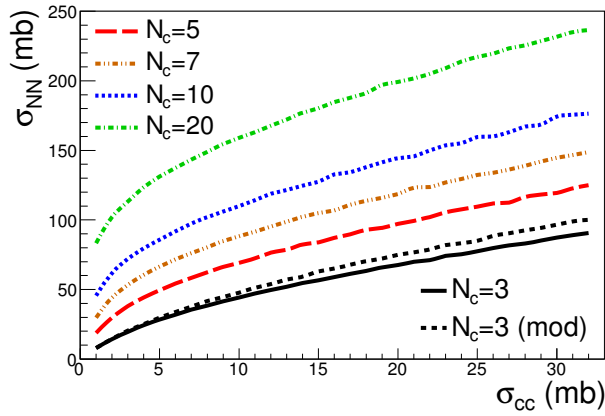


FIG. 6: Calculated σ_{NN} for various choices of N_c versus σ_{cc} .

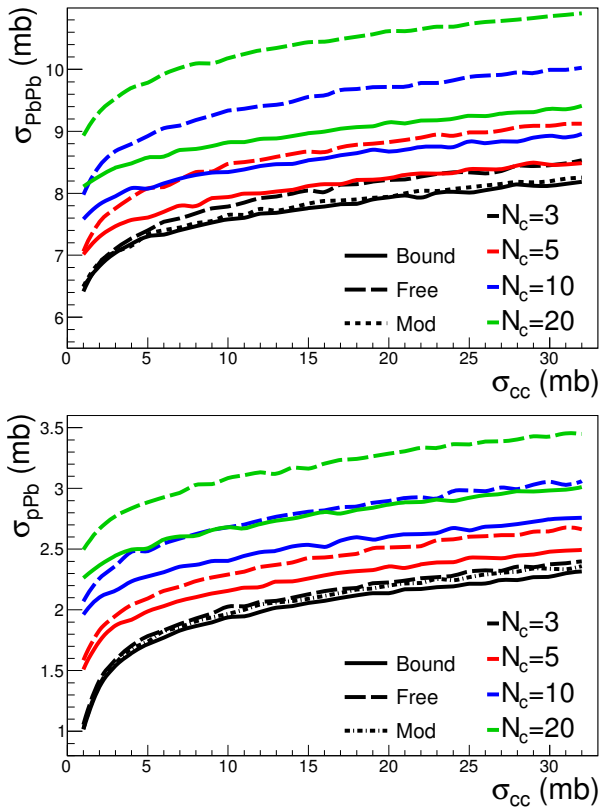


FIG. 7: Calculated total cross section for PbPb (top) and pPb (bottom) collisions for various choices of N_c versus σ_{cc} for the bound and free cases.

constituents. Figure 6 shows the dependence of σ_{NN} on σ_{cc} for various choices of N_c . As expected, σ_{NN} strongly increases with increasing σ_{cc} and N_c . For $N_c = 3$, the two parameterizations lead to a small but noticeable difference on σ_{NN} for $\sigma_{cc} \gtrsim 10$ mb. Figure 7 shows the increase of the PbPb (top) and pPb (bottom) cross sections with σ_{cc} for different values of N_c and the two ways to distribute the constituents, e.g. bound to nucleons or

N_c	σ_{cc} (mb)	μ	ν	σ_{NN} (mb)	σ_{PbPb} (b)	σ_{PbPb}^{free} (b)
3	18	3.4	2.6	63.3	7.83	8.15
3*	18	3.2	2.3	70.3	7.90	
5	10	4.3	3.6	69.1	7.94	8.47
7	5.5	4.8	3.9	69.0	7.92	8.52
10	3	5.4	4.2	72.1	7.95	8.68
3	14.4	3.3	2.3	55.4	7.74	
3*	11.9	3.0	2.0	53.6	7.71	
3	8.8	3.0	1.9	40.9	7.74	
5	6.4	3.9	2.8	55.8	7.75	
5	2.9	3.1	1.9	37.2	7.76	
10	1.7	4.4	2.9	56.8	7.78	

TABLE III: Values for PbPb collisions at $\sigma_{NN} = 5.02$ TeV. Input parameters are N_c , σ_{cc} and the way the constituents are distributed (bound, modified and free). Output values are $\mu = \langle N_{cpart} \rangle$, $\nu = \langle N_{ccoll} \rangle$, σ_{NN} and σ_{PbPb} as well as σ_{PbPb}^{free} for the freely distributing case. The modified cases are indicated with *. The parameters in rows above the horizontal line attempt to match $\sigma_{NN} = 70$ mb, while those below the horizontal line to match $\sigma_{PbPb} = 7.7$ b.

N_c	σ_{cc} (mb)	μ	ν	σ_{NN} (mb)	σ_{AuAu} (b)	σ_{AuAu}^{free} (b)
3	6	2.7	1.7	31.9	6.89	7.01
3*	6	2.6	1.6	33.9	6.91	
5	2.5	3.0	1.8	33.9	7.01	7.16
3	3.6	2.5	1.4	22.4	6.65	
3*	3.8	2.5	1.4	24.1	6.67	
3	3.2	2.5	1.4	20.5	6.66	
5	1.4	2.6	1.5	23.2	6.70	

TABLE IV: Values for AuAu collisions at $\sigma_{NN} = 19.6$ TeV, with $\sigma_{NN} = 33$ mb and $\sigma_{AuAu} = 6.7$ b. See description in Tab. III for more information.

freely distributed inside the nucleus. For the same parameters, the freely-distributing case always leads to a larger cross section than the bound case. In particular, for large σ_{cc} and N_c the likelihood for peripheral collisions to occur increases significantly, making the total cross section exceed the value expected from geometrical considerations (also visible in the right panel of Fig. 5). For example, 8 b corresponds to an effective radius of about 8 fm (which is larger than $R + 2a$ of Pb).

In the following section, results will be discussed where the parameters for the calculation are chosen to approximately reflect PbPb collisions at $\sqrt{s_{NN}} = 5.02$ TeV, and AuAu collisions at $\sqrt{s_{NN}} = 19.6$ GeV, respectively. The calculations are performed for various choices of N_c and σ_{cc} , as well as various ways to distribute the constituents, i.e. bound, modified and free cases. The parameters, which are summarized in Tab. III and Tab. IV, have been set to roughly match the corresponding σ_{NN} and the total σ_{PbPb} , respectively.

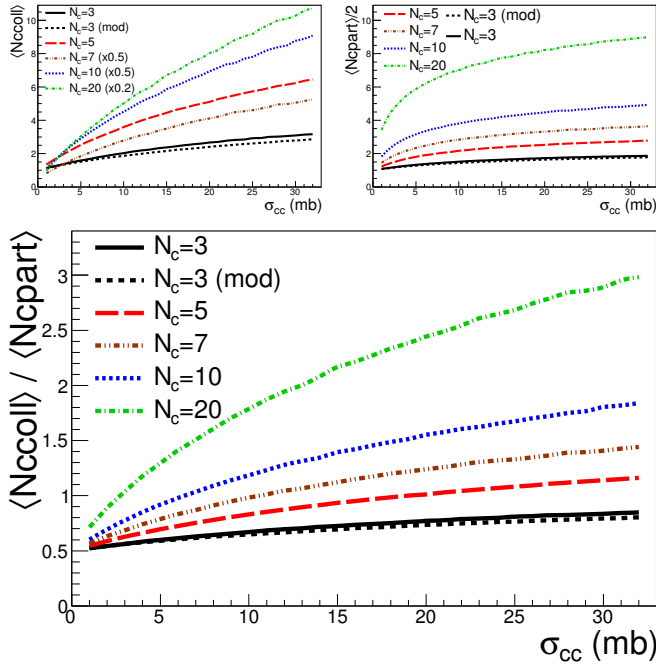


FIG. 8: Average values of N_{ccoll} (top left) and N_{cpart} (top right panel), as well as of the ratio $N_{\text{ccoll}}/N_{\text{cpart}}$ (bottom panel) versus σ_{cc} for various N_c in pp collisions.

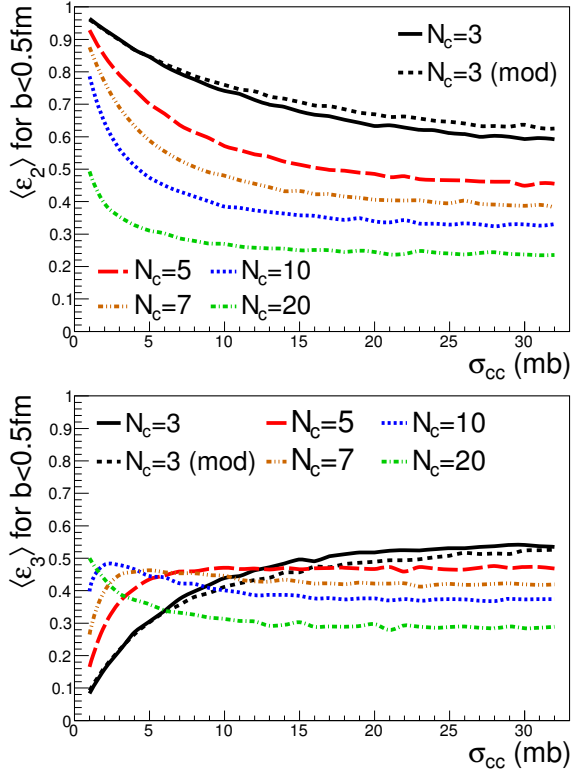


FIG. 9: Average eccentricity (top) and triangularity (bottom) for $b < 0.5$ fm versus σ_{cc} for various N_c in pp collisions.

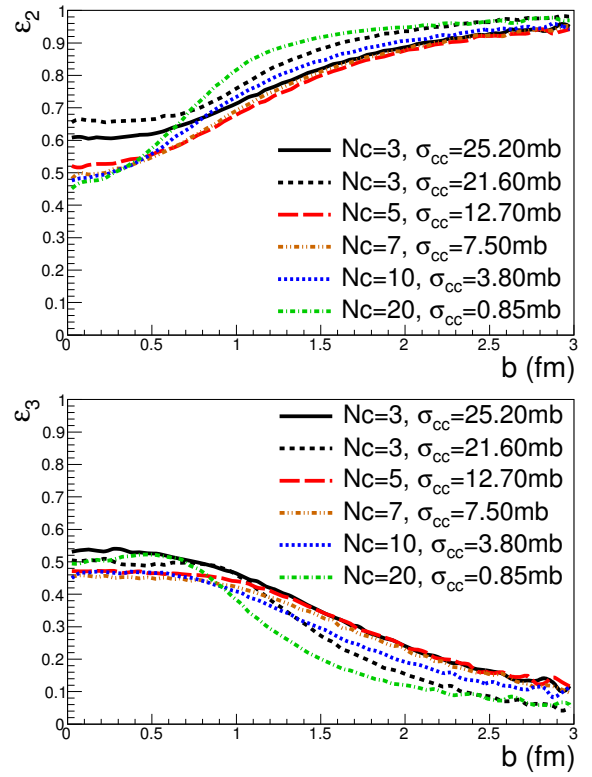


FIG. 10: Average eccentricity (top) and triangularity (bottom) versus b for various N_c in pp collisions at 13 TeV. The calculation for $\sigma_{\text{cc}} = 21.60$ mb corresponds to the modified case.

IV. RESULTS

In this section, results of constituent Glauber model calculations are presented for various input parameters and collision systems.

A. pp collisions

Figure 8 shows average values of N_{ccoll} and N_{cpart} , as well as of the ratio $N_{\text{ccoll}}/N_{\text{cpart}}$ versus σ_{cc} for various N_c in pp collisions. The resulting values increase with increasing N_c and σ_{cc} compared to those at nucleon level, which are $N_{\text{part}} = 2$, $N_{\text{coll}} = 1$, and $N_{\text{coll}}/N_{\text{part}} = 0.5$.

Figure 9 shows the dependence of the average eccentricity $\langle \varepsilon_2 \rangle$ and triangularity $\langle \varepsilon_3 \rangle$ versus σ_{cc} for various N_c in central pp collisions with $b < 0.5$ fm. Increasing N_c and σ_{cc} decreases the observed initial-state anisotropy as expected for a spherically symmetric system. Figure 10 shows eccentricity and triangularity versus b for a set of input parameters reflecting pp collisions at 13 TeV. For central collisions ($b < 0.5$ fm) $0.45 < \varepsilon_2 < 0.65$ and $0.46 < \varepsilon_3 < 0.54$ leading to scaled values of about 0.1 and 0.02 for measured values [30, 31] of $v_2 \sim 0.05$ and $v_3 \sim 0.01$, respectively.

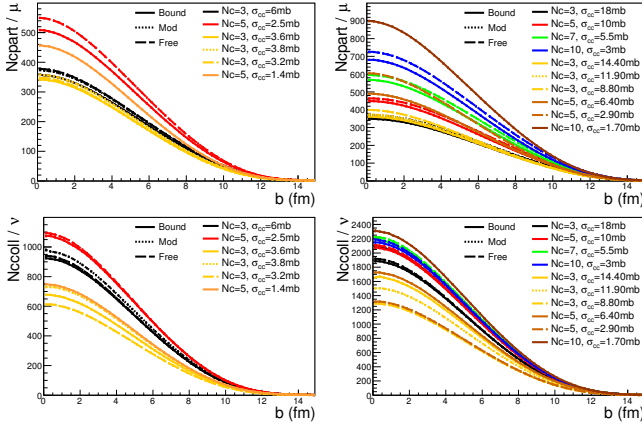


FIG. 11: N_{cpart}/μ (top) and N_{ccoll}/ν (bottom panels) for AuAu (left) and PbPb (right panels) collisions. The parameters for the calculations are summarized in Tab. III and Tab. IV.

B. AA collisions

The results for AA collisions, discussed in this section, are obtained for calculations where the parameters are chosen to approximately reflect PbPb collisions at $\sqrt{s_{\text{NN}}} = 5.02$ TeV, and AuAu collisions at $\sqrt{s_{\text{NN}}} = 19.6$ GeV, respectively. The parameters are summarized in Tab. III for PbPb and Tab. IV for AuAu collisions. Figure 11 shows N_{cpart}/μ and N_{ccoll}/ν versus b , where $\mu = \langle N_{\text{cpart}} \rangle$ and $\nu = \langle N_{\text{ccoll}} \rangle$ in pp collision, respectively. Figure 12 shows the ratio $N_{\text{cpart}}/N_{\text{part}}$ versus N_{part} normalized to $\mu/2$. The calculations are performed in small bins of b and then matched to the corresponding N_{part} at nucleon level, since in peripheral events $\langle N_{\text{part}} \rangle$ for events selected with $N_{\text{cpart}} > 0$ slightly differs from those calculated at nucleon level and selected with $N_{\text{part}} > 0$. In particular for $N_c \leq 5$, the shape is similar to that of the measured $2dN/d\eta/N_{\text{part}}$ [21, 32, 33]. The inverse of what is plotted, i.e. $\mu/2N_{\text{part}}/N_{\text{cpart}}$, would be the factor needed to translate the measurements scaled by $N_{\text{part}}/2$ to N_{cpart}/μ . Hence, as can be seen from the figure, the correction would affect the shape the strongest for peripheral events, making $\mu dN/d\eta/N_{\text{cpart}}$ approximately flat.

Particle production in central AA collisions scaled by N_{part} compared to that in inelastic pp collisions turned out to rise stronger with collision energy, with $s_{\text{NN}}^{0.155}$ rather than $s_{\text{NN}}^{0.103}$, respectively [33]. To evaluate if normalizing by constituent instead of nucleon participants would lead to a more similar behavior, the ratio N_{cpart}/μ has been computed for various N_c and several ways to distribute the sub-nuclear degrees of freedom. The computed ratios for $b < 3.5$ fm are shown versus $\sqrt{s_{\text{NN}}}$ in Fig. 13, and found to slightly decrease with increasing $\sqrt{s_{\text{NN}}}$. This trend can be compared to data, using the ratio of the power-law fits to the central AA and the inelastic pp data taken from Ref. [33]. The ratio of the

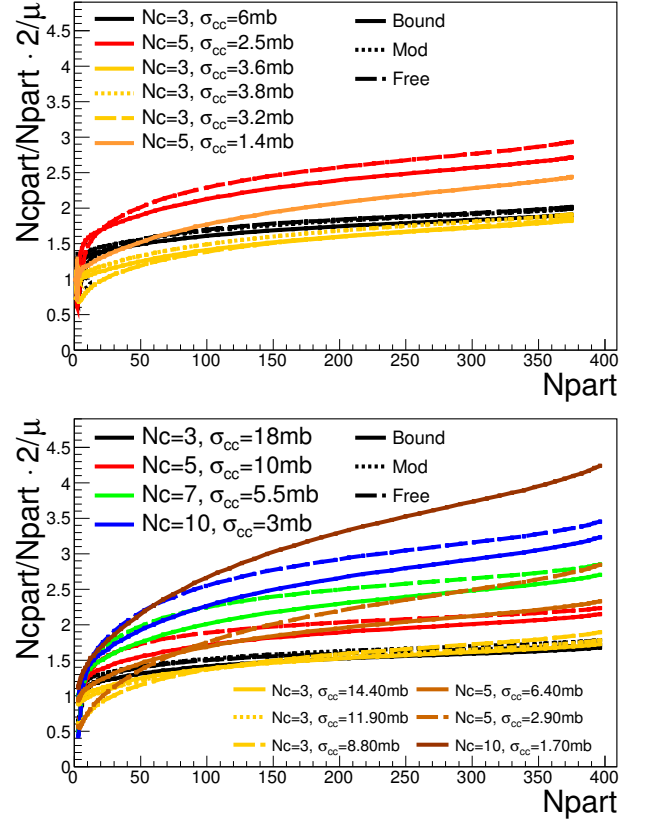


FIG. 12: Ratio $N_{\text{cpart}}/N_{\text{part}}$ normalized to $\mu/2$ for AuAu (top) and PbPb (bottom panel) collisions. The parameters for the calculations are summarized in Tab. III and Tab. IV.

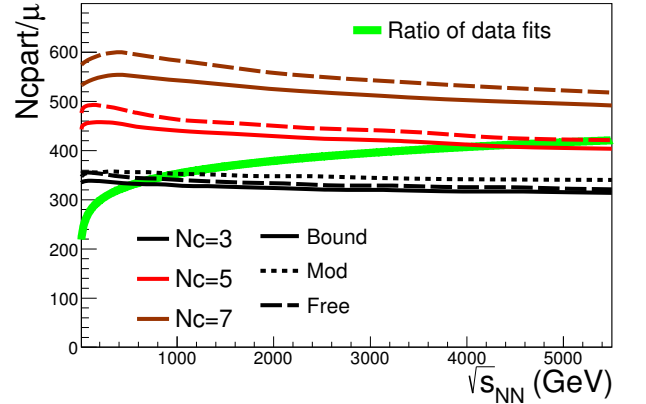


FIG. 13: Ratio of fits to central AA (scaled by 160 to approximately account for $N_{\text{part}}/2$) and inelastic pp collisions compared to N_{cpart}/μ from constituent Glauber calculations for $b < 3.5$ fm. The values for the power law fits are taken from [33].

power-law fits is scaled by 160 to roughly account for normalizing the central AA data by $N_{\text{part}}/2$, since for central AuAu at $\sqrt{s_{\text{NN}}} = 19.6$ GeV $N_{\text{part}} \approx 340$, while $N_{\text{part}} \approx 385$ for PbPb at $\sqrt{s_{\text{NN}}} = 5.02$ TeV. As can be

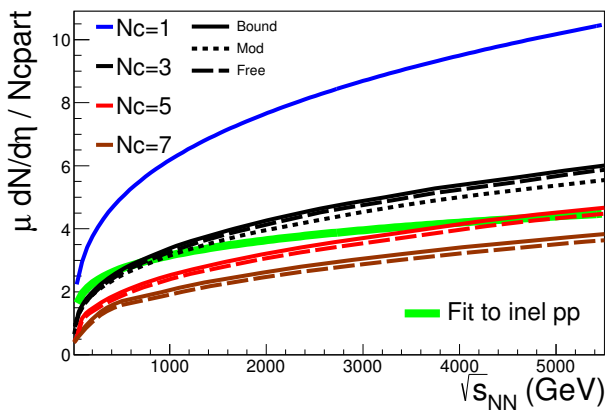


FIG. 14: Power-law fit of $dN/d\eta$ from inelastic pp collisions compared to scaled central AA data. The AA curves are obtained from a power-law fit to $2dN/d\eta/N_{\text{part}}$ scaled by μ/N_{cpart} (multiplied by 160 to approximately account for $N_{\text{part}}/2$) for constituent Glauber calculations with $b < 3.5$ fm. In the case of $N_c = 1$, $N_{\text{cpart}} = N_{\text{part}}$ and $\mu = 2$, the shown curve essentially represents the original fit to $2dN/d\eta/N_{\text{part}}$. The values for the power law fits are taken from [33].

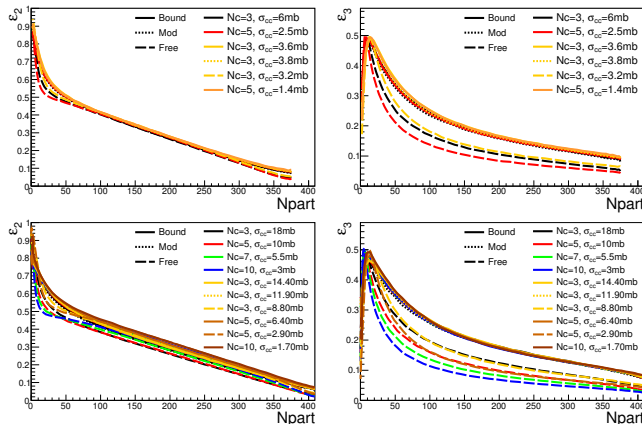


FIG. 15: Eccentricity (left) and triangularity (right panels) for AuAu (top) and PbPb (bottom panels) collisions. The parameters for the calculations are summarized in Tab. III and Tab. IV.

seen in the figure, the data exhibit a different trend, i.e. the ratio is slightly rising with $\sqrt{s_{\text{NN}}}$. The comparison between data and calculations does not reveal a preferred value for N_c . At lower energy $N_c = 3$, while at higher energy $N_c = 5$ is supported by the data, indicating that the

number of relevant partonic degrees of freedom increase with increasing collision energy. On an absolute scale, Figure 14 indeed confirms that scaling with N_{cpart}/μ for $N_c = 3$ or 5 leads to a more similar collision energy dependence of central AA and inelastic pp data than based on N_{part} (labeled with $N_c = 1$).

Figure 15 shows the eccentricity and triangularity versus N_{part} calculated for parameters given in Tab. III and Tab. IV, and are quite similar to those calculated from participant nucleons. The triangularity exhibits a stronger variation to changes of the calculation than the eccentricity, which is found to be quite insensitive to the actual values of the parameters. As for the case of nuclear participant calculation [34], ε_2 and ε_3 differ only by about 10 % for ultra-central collisions.

V. SUMMARY

Glauber models based on nucleon–nucleon interactions are commonly used to calculate properties of the initial state in high-energy nuclear collisions, and their dependence on impact parameter or number of participating nucleons. Such calculations have been extended to sub-nucleon level by taking into account three valence quarks per nucleon in the scattering process. In particular, it has been shown that particle production at mid-rapidity in high-energy nucleus–nucleus collisions scales almost linearly with the number of quark participants. In this article, an extension of the Glauber model to any number of constituents is presented. Properties of the initial state, such as the number of constituent participants and collisions, as well as eccentricity and triangularity, are calculated and systematically compared for different assumptions to distribute the sub-nuclear degrees of freedom and for various collision systems. The code for the constituent Monte Carlo Glauber program is made publicly available. The author welcomes comments on the code and suggestions on how to make it more useful to both experimentalists and theorists.

Acknowledgments

I would like to thank J.Schukraft and S.Sorensen for interesting discussions. This work is supported in part by the U.S. Department of Energy, Office of Science, Office of Nuclear Physics, under contract number DE-AC02-05CH11231.

[1] M. L. Miller, K. Reygers, S. J. Sanders, and P. Steinberg, *Ann. Rev. Nucl. Part. Sci.* **57**, 205 (2007), [arXiv:nucl-ex/0701025](#).
 [2] A. Bialas, M. Bleszynski, and W. Czyz, *Nucl. Phys.* **B111**, 461 (1976).

[3] K. J. Eskola, K. Kajantie, and J. Lindfors, *Nucl. Phys.* **B323**, 37 (1989).
 [4] B. Alver, M. Baker, C. Loizides, and P. Steinberg (2008), [arXiv:0805.4411](#).
 [5] M. Rybczynski, G. Stefanek, W. Broniowski, and

- P. Bozek, *Comput. Phys. Commun.* **185**, 1759 (2014), [arXiv:1310.5475](#).
- [6] S. Eremín and S. Voloshin, *Phys. Rev.* **C67**, 064905 (2003), [arXiv:nucl-th/0302071](#).
- [7] S. S. Adler et al. (PHENIX), *Phys. Rev.* **C89**, 044905 (2014), [arXiv:1312.6676](#).
- [8] A. Adare et al. (2015), [arXiv:1509.06727](#).
- [9] R. A. Lacey, P. Liu, N. Magdy, M. Csanád, B. Schweid, N. N. Ajitanand, J. Alexander, and R. Pak (2016), [arXiv:1601.06001](#).
- [10] L. Zheng and Z. Yin, *Eur. Phys. J.* **A52**, 45 (2016), [arXiv:1603.02515](#).
- [11] C. Loizides (2016), 1602.09138.
- [12] B. Alver et al., *Phys. Rev.* **C77**, 014906 (2008), [arXiv:0711.3724](#).
- [13] H. De Vries, C. W. De Jager, and C. De Vries, *Atom. Data Nucl. Data Tabl.* **36**, 495 (1987).
- [14] Q. Y. Shou, Y. G. Ma, P. Sorensen, A. H. Tang, F. Videbæk, and H. Wang, *Phys. Lett.* **B749**, 215 (2015), [arXiv:1409.8375](#).
- [15] C. Loizides, J. Nagle, and P. Steinberg (2014), [arXiv:1408.2549](#).
- [16] D. A. Fagundes, M. J. Menon, and P. V. R. G. Silva, *J. Phys.* **G40**, 065005 (2013), [arXiv:1208.3456](#).
- [17] B. Abelev et al. (ALICE), *Phys. Rev.* **C88**, 044909 (2013), [arXiv:1301.4361](#).
- [18] J. Adam et al. (ALICE), *Phys. Rev.* **C91**, 064905 (2015), [arXiv:1412.6828](#).
- [19] B. Abelev et al. (ALICE), *Phys. Rev. Lett.* **109**, 252302 (2012), [arXiv:1203.2436](#).
- [20] V. Khachatryan et al. (CMS) (2015), [arXiv:1509.03893](#).
- [21] B. Alver et al. (PHOBOS), *Phys. Rev.* **C83**, 024913 (2011), [arXiv:1011.1940](#).
- [22] M. M. Aggarwal et al. (WA98), *Phys. Rev. Lett.* **85**, 3595 (2000), [arXiv:nucl-ex/0006008](#).
- [23] S. S. Adler et al. (PHENIX), *Phys. Rev. Lett.* **94**, 232301 (2005), [arXiv:nucl-ex/0503003](#).
- [24] S. Chatrchyan et al. (CMS), *Phys. Lett.* **B710**, 256 (2012), [arXiv:1201.3093](#).
- [25] B. Alver et al. (PHOBOS), *Phys. Rev. Lett.* **98**, 242302 (2007), [arXiv:nucl-ex/0610037](#).
- [26] B. Alver and G. Roland, *Phys. Rev.* **C81**, 054905 (2010), [Erratum: *Phys. Rev.* **C82**, 039903(2010)], [arXiv:1003.0194](#).
- [27] D. Teaney and L. Yan, *Phys. Rev.* **C83**, 064904 (2011), [arXiv:1010.1876](#).
- [28] D. d’Enterria, G. K. Eyyubova, V. L. Korotkikh, I. P. Lokhtin, S. V. Petrushanko, L. I. Sarycheva, and A. M. Snigirev, *Eur. Phys. J.* **C66**, 173 (2010), [arXiv:0910.3029](#).
- [29] R. Hofstadter, *Rev. Mod. Phys.* **28**, 214 (1956).
- [30] G. Aad et al. (ATLAS) (2015), [arXiv:1509.04776](#).
- [31] V. Khachatryan et al. (CMS), *CMS-PAS-FSQ-15-002* (2015).
- [32] K. Aamodt et al. (ALICE), *Phys. Rev. Lett.* **106**, 032301 (2011), [arXiv:1012.1657](#).
- [33] J. Adam et al. (ALICE) (2015), [arXiv:1512.06104](#).
- [34] C. Shen and U. Heinz (2015), [arXiv:1507.01558](#).
- [35] R. Brun and F. Rademakers, *Nucl. Instrum. Meth.* **A389**, 81 (1997).
- [36] J. D. Bjorken, *Phys. Rev.* **D27**, 140 (1983).

Appendix A: Program code

The program code, called “runCGM.C”, for the generalized constituent Monte Carlo Glauber can be found at <http://tglaubermc.hepforge.org/svn/branches/tools/runCGM.C>. It requires “runGlauber_v2.3.C” from the most recent TGlauberMC version (v2.3) [15], which can be downloaded from from HepForge (<http://www.hepforge.org/downloads/tglaubermc>), and ROOT [35] (see <http://root.cern.ch> for installation files and documentation.). To compile the code, execute at the ROOT prompt:

```
.L runGlauber_2.3.C+
.L runCGM.C+
```

The function “runCGM” can be run with the following arguments:

```
Int_t n           = number of events
const char *sysA  = system A
const char *sysB  = system B
Double_t signn    = NN cross section (mb)
Double_t mind     = min. dist. betw. nucleons
Int_t nc         = number of constituents / dof
Double_t sigcc    = constituent cross section (mb)
Int_t type,      -> how to distribute dof:
                  =0 no recentering
                  =5 modified (PHENIX)
                  =8 free no recentering
const char *fname = output filename
Double_t bmin     = min. imp. parameter
Double_t bmax     = max. imp. parameter
```

The output ROOT “ntuple” contains the following list of per-event variables:

```
Npart  = number of nucleon participants
Ncoll  = number of nucleon collisions
B      = impact parameter
Ncpart = number of constituent participants
Nccoll = number of constituent collisions
Ap     = area def. by participant (co-)variances
Ac     = area def. by constituent (co-)variances
EccXP  = eccX nucleon participants (X=1-5)
EccXC  = eccX constituent participants (X=1-5)
```

All distributions discussed in Sec. IV have been obtained from the output of “runGCM”.

Appendix B: Area calculation

As briefly mentioned in Sec. II, the overlap area of two colliding nuclei is usually taken to be proportional to $S = \sqrt{\sigma_x^2 \sigma_y^2 - \sigma_{xy}^2}$, given by the (co-)variances of the participant distributions in the transverse plane [12]. However, using the participant distributions does not provide a direct measure of the area, and in particular misses

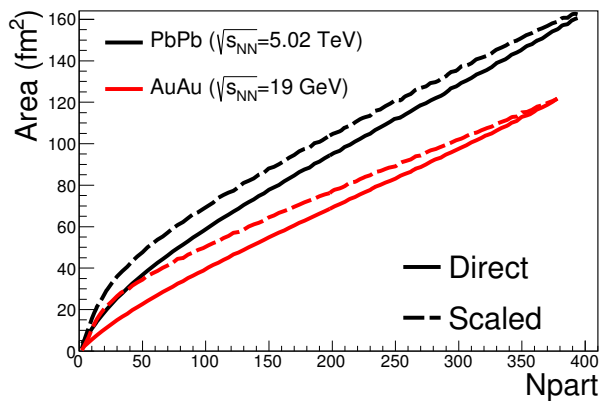


FIG. 16: Area calculated directly by counting of the overlap area and scaled using the participant widths for AuAu collisions at $\sqrt{s_{NN}} = 19$ GeV and PbPb collisions at $\sqrt{s_{NN}} = 5.02$ TeV.

also the absolute normalization. Instead, one can event-by-event compute the overlap area directly using a fine-grained grid. Figure 16 compares the two approaches for AuAu collisions at $\sqrt{s_{NN}} = 19$ GeV and PbPb collisions at $\sqrt{s_{NN}} = 5.02$ TeV, where the results using the participant widths were rescaled by A_0/S_0 where S_0 and the absolute area A_0 were obtained at $b = 0$ fm. The values are $S_0 = 9.8$ and 8.7 with RMS of 0.4 , and $A_0 = 165.8$ and 120.1 with RMS of 5.2 and 3.9 for PbPb and AuAu, respectively (all units in fm^2). The code can be found at <http://tglaufermc.hepforge.org>.

[org/svn/branches/tools/runArea.C](http://svn/branches/tools/runArea.C).

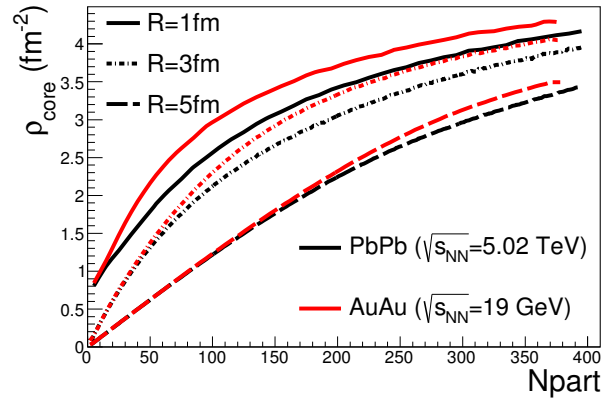


FIG. 17: Participant transverse area density in an area given by radius $R = 1, 3$ and 5 fm for AuAu collisions at $\sqrt{s_{NN}} = 19$ GeV and PbPb collisions at $\sqrt{s_{NN}} = 5.02$ TeV.

Alternatively, instead of directly using the area when estimating the energy density via the Bjorken estimate [36], one can use the participant transverse area density, ρ_{core} , which can be obtained by counting the number of participants within a core area of given radius R . Figure 17 shows ρ_{core} for various choices of R in AuAu collisions at $\sqrt{s_{NN}} = 19$ GeV and PbPb collisions at $\sqrt{s_{NN}} = 5.02$ TeV. The code can be found at <http://tglaufermc.hepforge.org/svn/branches/tools/runCore.C>